published by Ural Federal University
eISSN 2411-1414
chimicatechnoacta.ru

ARTICLE
2024, vol. 11(3), No. 202411301
DOI: 10.15826/chimtech.2024.11.3.01

Assessment of different crosslinking mechanisms on PVA-based membranes to achieve water resistance with iron imprinting sites

Ihsan Alfikro [ab], Jorena [ab], Octavianus Cakra Satya [a], Erry Koriyanti [a], Fiber Monado [a], Idha Royani [ab] *

a: Department of Physics, Faculty of Mathematics and Natural Science, Sriwijaya University, Indralaya 30662, Indonesia
b: Laboratory of Material Science, Faculty of Mathematics and Natural Science, Sriwijaya University, Indralaya 30662, Indonesia
* Corresponding author: idharoyani@unsri.ac.id

This paper belongs to a Regular Issue.

Abstract

Water-resistant PVA (polyvinyl alcohol) electrospun membranes with different crosslinking mechanisms were synthesized using the facile electrospinning technique. The crosslinking mechanisms were differentiated by introducing 2 different functional groups of different crosslinker agents into the molecular structure of the membrane. The evaluation of water resistance was conducted by both micro- and macro-structural analyses, such as Fourier Transform Infrared spectroscopy (FTIR), Scanning Electron Microscope (SEM), Energy Dispersive X-ray Spectroscopy (EDS), X-ray Diffraction (XRD), water contact angle (WCA), and immersion test. Infrared spectra confirmed the formation of new bands at around 1700 cm^{-1}, which are acetal or ester groups, indicating the successful crosslinked process. Additionally, the lowered intensity of hydroxyl groups also signifies that the membrane is water-resistant. The XRD patterns showed the signature peak of PVA at the angle of 20°. Furthermore, the reduction in iron content, as shown by EDS spectra, was attributed to the surface imprinting process. SEM images displayed the formation of nanofibers, with mean diameters of 103 nm and interconnecting nanobead structures. The results showed that WCA was significantly enhanced, up to 91°, with minor loss in structure during water immersion test for 24 h. These findings confirm the hydrophobic characteristics of the membranes and their potential application in water-related fields.

Keywords

poly(vinyl) alcohol
surface imprinting
water resistant
crosslinking
electrospinning

Received: 22.05.24
Revised: 11.06.24
Accepted: 17.06.24
Available online: 25.06.24

Key findings

- Formation of acetal and ester groups, as the main crosslinking mechanism, lead to hydrophobic characteristics.
- Crosslinking mechanism provides more amorphous regions to the membrane.
- Lower solution viscosity lead to the formation of nanobeads, initiated by electrospraying process.

1. Introduction

Water is an important factor that sustains life in various environments, constituting approximately ±60% of the body mass in most living organisms, including humans. However, water often becomes a carrier for various dangerous substances or pollutants due to advancements in industries, including organic dyes, pathogenic substances, heavy metals, and persistent organic pollutants [1–4]. Among the pollutants, heavy metals are a group of potentially toxic substances that cannot be easily decomposed and tend to accumulate in the body. These metals are naturally present in rivers, lakes, and seas, making water the primary medium for environmental accumulation [5]. A study conducted by Ugaz et al. [6] at an abandoned mining site in Spain showed severe pollution in the surrounding river despite the cessation of

mining activities for a century. Metals, such as As, Co, Cr, Cu, Fe, Ni, and Pb, were identified as the main contaminants, exceeding allowed thresholds.

A similar study was conducted by Kamarati et al. [7], where water samples were collected at 3 different points from the Santan River in East Kalimantan before and after the rain. All samples were at concerning pollution levels due to dissolved iron exceeding the established quality standards [8], specifically at the second point, which had surpassed 1 mg/L, due to its close proximity to the coal mine. Another investigation by Rusydi et al. [9] focused on the dissolved iron content in 28 different groundwater sources in the Indramayu area of West Java. The results showed that the average content was 10.3 mg/L, with 40% of the total samples contaminated due to human activities.

To address the issue, the implementation of a water treatment system to purify iron contamination is necessary. Adsorption technique is most often adopted [10], utilizing an adsorbent capable of not only adsorbing pollutants but also serving as a sensor, thereby enhancing the selectivity towards certain contaminants. An effective approach to achieving this is by surface imprinting [11, 12]. The process includes printing a template of metal ions on the surface of a material to increase its affinity [13]. Several studies were conducted to explore and implement the method, as detailed in Table 1.

The utilization of nanofiber-based membranes synthesized using the electrospinning method shows the potential for reusability and high porosity [18, 19] in a sustainable ferrous metal adsorption process. PVA, a polymer widely used for the synthesis of nanofibers, is known to be nontoxic and biodegradable due to its abundant hydroxyl content. These qualities make the polymer environmentally friendly and compatible for use as an adsorption membrane [20]. However, hydrogen bonds may occur between hydroxyl groups and water, leading to the high solubility of PVA [21]. Various recent studies [22–25] succeeded in overcoming this problem by modifying the molecular structure through a crosslinking process.

The study focuses on modifying the structure of the PVA combined with a natural polymer, gelatin (GE), for membrane fabrication using 2 different crosslinker agents, namely citric acid (CA) and glutaraldehyde (GA). These agents have different mechanisms for forming waterproof or hydrophobic membranes.

Table 1 Surface imprinting method on various polymer-based adsorbents.

Polymer	Imprinting agent	Target	Ref.
Cellulose	HNO_3+EDTA	Pb^{2+}	[14]
PEG-2000	HCl	Cd^{2+}	[13]
PMAA	HCl	Pb^{2+}	[15]
Sericin/PVA	HCl	Methylene blue	[16]
Chitosan	HCl	Pb^{2+}	[17]
PVA/Gelatin	HCl	Fe^{3+}	This study

The crosslinking mechanism was observed through FTIR characterization to determine the group responsible for imparting the hydrophobic properties of the membrane, followed by macro-testing through the measurement of contact angle and water immersion test. Membrane morphology was examined through SEM characterization along with elemental assessment and EDS analysis. Additionally, the crystallinity of the membrane was assessed by X-ray diffraction analysis.

2. Experimental procedures

2.1. Materials

Low-molecular-weight poly(vinyl alcohol) (PVA) (approx. 10,000 Da), gelatin (porcine skin, type A), ferric nitrate nonahydrate ($Fe(NO_3)_3.9H_2O$), acetic acid (CH_3COOH) glacial 100%, hydrochloric acid (HCl) 37%, glutaraldehyde 25% in water, and acetone (CH_3COCH_3) were bought from Sigma-Aldrich Chemical Reagent Co., with high purity (>99%). High-hydrated citric acid ($C_6H_8O_7$) and analytical grade deionized water (H_2O) with a purity of 99% were obtained from Kimia Market (Bandung, Indonesia) and OneMed (Surabaya, Indonesia), respectively. All chemicals were used without any further purification.

2.2. Synthesis of PVA/GE 15/5 wt.% membrane

Gelatin (5% w/v) was dissolved in a solvent comprised of acetic acid and water in a 1:10 ratio at room temperature until complete dissolution. Subsequently, PVA powder (15% w/v) was added, and the mixture was stirred at 85 °C to obtain a PVA/GE 15/5 wt.% homogenous solution. During continuous stirring, 200 mg of the template imprinting salt, $Fe(NO_3)_3.9H_2O$, was introduced, changing the solution to yellowish-clear in color. Finally, 1 g of citric acid powder was added to initiate the crosslinking process. A similar procedure was conducted without the addition of citric acid.

The electrospinning process was conducted under identical parameters for both solutions, including an operating voltage of 16 kV, an 18G blunt needle, a 12 cm needle-collector distance, an injector rate of 0.4 mL/h, and a chamber relative humidity of 50%, passively controlled by silica gel. The collected membranes were dried overnight in a desiccator to vaporize the excess solvent.

The crosslinking mechanism of a citric acid (CA)-composed membrane, named PVA/GE 15/5 wt.% ~ CA, was activated by heating at 170 °C for 10 minutes. This changed the clean-white membrane to a slightly yellow color. A mixture of glutaraldehyde and acetone (1:50) was used to immerse the CA-free membrane, labelled PVA/GE 15/5 wt.% ~GA, for 2 h at a controlled pH of 2 using 1 M HCl. Finally, the membranes were washed with 1 M HCl several times to trigger the imprinting of Fe^{3+} sites on the surface before being dried in the desiccator.

 DOI: 10.15826/chimtech.2024.11.3.01

2.3. Characterization

The main aspect of the crosslinked process was observed by determining the modified molecular chain interaction of each functional group using a Fourier Transform Infrared spectrophotometer (type IR Prestige-21 SHIMADZU) within the wavenumber range of 4000–500 cm^{-1}. The morphology of the membrane was observed by a Scanning Electron Microscope (SEM type VEGA3 TESCAN) operating at 15 kV operating voltage, equipped with an X-ray detector to analyze elemental composition by Energy Dispersive X-ray Spectroscopy (EDS spectra ~20 keV; Bruker). Crystallinity was characterized using X-ray diffraction (XRD; Rigaku Miniflex 600 series) at room temperature through Cu Kα radiation. The measurements were conducted at a scanning rate of 10°/min in the 2-theta angle range of 5–60°. Data refinement was conducted using the Rietveld method with Profex 5.2.4 software to determine the crystal phase and peak position [26]. Additionally, the water contact angle of the membrane was photographed using a 5 MP camera at f/2.4 (macro configuration) and analyzed by ImageJ 1.54f, assisted by Drop Analysis LB-ADSA (Low Bond Axisymmetric Drop Shape Analysis) plugin [27].

3. Results and Discussions

3.1. Molecular chain and crosslinking mechanisms

Figure 1 shows the FTIR spectra for uncrosslinked, citric acid (CA)-crosslinked, and glutaraldehyde (GA)-crosslinked membranes, respectively. All samples showed similar absorption bands without significant changes. This signified the absence of an adverse impact on the primary polymer structure of the membranes [28]. The broad absorption band at 3500–3200 cm^{-1} corresponded to the stretching of the hydroxyl group, –OH, indicating intramolecular hydrogen bonds within the membrane [29]. Since hydroxyl groups form hydrogen bonds with water molecules, reducing the absorbance of these groups during the crosslinking process was crucial for enhancing the membrane's waterproof properties [30].

The absorption at 2925 cm^{-1} suggested the C–H stretching of the alkyl group, followed by the CH_2 bending vibration at 1427 cm^{-1} and the stretching bond of C–C at 848 cm^{-1} which all indicate the characteristic bands of PVA [31, 32]. The main indication of the presence of gelatin was the absorption band of the amide group at 1700–1200 cm^{-1}. This comprised amide I (1700–1600 cm^{-1}), amide II (1575–1480 cm^{-1}), and amide III (1330–1230 cm^{-1}), showing C=O, N–H, and C–N stretchings, respectively [33, 34].

The crosslinking mechanism by glutaraldehyde was observed in the acetalization process of the reaction between alcohol and the aldehyde group at 1700–1600 cm^{-1}, which signifies the C=O functional group [35]. However, the addition of gelatin makes observations difficult because the absorption bands coincide with the amide groups.

Acetalization was observed by decreasing and narrowing the absorption of the hydroxyl group as it reacted with the aldehyde group to form acetal, as shown in Figure 2. According to Huang et al. [36], the formation of acetal can also be observed at wavenumbers 1140–1000 cm^{-1}, signifying the broadening of the –OCO– functional group after being GA-crosslinked. This broadening exhibited a 27% increase compared to what was before the crosslinking process in the 1141 cm^{-1} band.

A different mechanism was demonstrated by CA-crosslinking, where the formation of an ester group occurred from the product between the carboxylic acid (–COOH) and alcohol (–OH) groups [37]. Figure 3 shows the infrared spectra at 4000–750 cm^{-1} of the membrane before and after being crosslinked by citric acid. A new band appears at ~1720 cm^{-1} in the CA-crosslinked membrane, signifying stretching of the C=O band [38]. This proved the existence of intermolecular chains between PVA and citric acid, indicative of ester formation [31, 39]. However, it is clearly seen that the hydroxyl groups before and after crosslinking overlap each other, leading to the conclusion that there is no decrease in the number of hydroxyl groups even after crosslinking, in contrast to that after esterification.

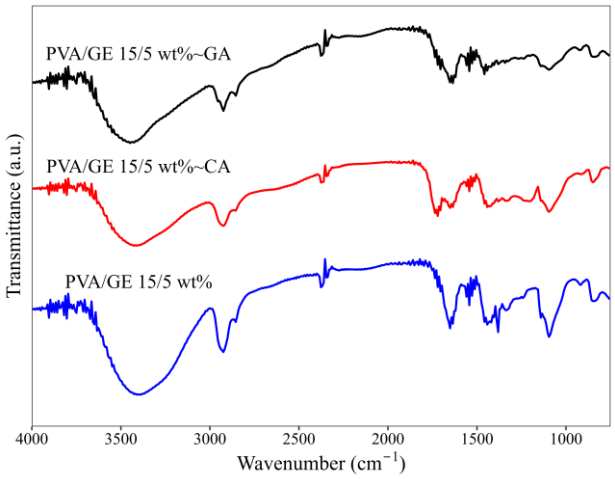

Figure 1 FTIR spectra of uncrosslinked membrane and crosslinked membranes.

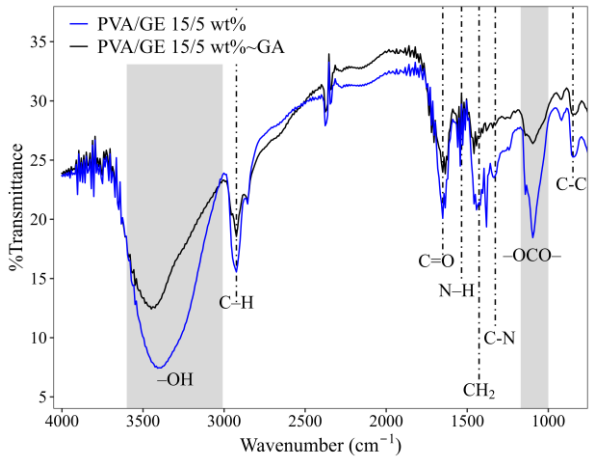

Figure 2 FTIR spectra of PVA/GE 15/5 wt.% membrane (blue) and PVA/GE 15/5 wt.%~GA membrane (black).

 DOI: 10.15826/chimtech.2024.11.3.01

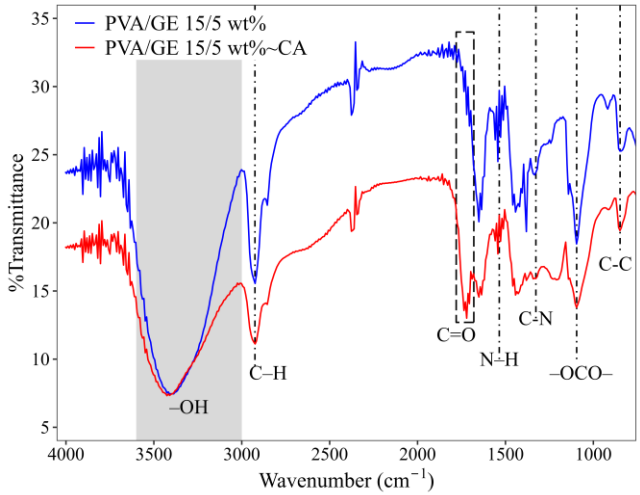

Figure 3 FTIR spectra of PVA/GE 15/5 wt.% membrane (blue) and PVA/GE 15/5 wt.%~CA membrane (red).

This might be due to the high hydration degree of citric acid used, so that the combination with polymers leads to the greater content of hydroxyl groups in CA-free membranes. Then, it is suggested to utilize anhydrous forms of citric acid for further study.

3.2. Membrane morphology and elemental analysis

The formation of nanofibers was determined by examining the surface morphology of the membrane under a microscope, specifically when the images were displayed at the nano/micron scale. SEM is a suitable option for visualizing the surface morphology of materials at high magnification and is equipped with elemental mapping capabilities.

Figure 4 shows the morphology and fiber distribution of the membrane with a magnification of up to 10,000 times, showing predominantly nanobead formation interconnected by thin fibers. The gradual evaporation of the solvent, facilitated by maintaining humidity at 50%, aided in elongating the solution under the applied voltage, leading to the formation of nanofiber structures on the collector due to the increased viscosity from evaporation. However, the membrane was dominated by the nanobead structure.

Insufficient viscosity could lead to nanobead formation, which is when solutions are sprayed instead of elongated, known as the electrospraying process. Both electrospraying and electrospinning methods were related to each other and shared the same parental event, referred to as electrohydrodynamics [40]. Figure 4a shows a fiber structure with a centralized diameter distribution below 100 nm, with a mean diameter of 103 nm. After the imprinting process, the membrane structure experienced deformation, as shown in Figure 4b, due to the influence of the acidity of HCl, thereby reducing the fibers formed but maintaining nanobead particle structure [17]. The number of fibers decreased drastically, with the average diameter slightly increasing and measured at 118 nm.

EDS spectra, as shown in Figure 5, present the concentrations of elements in the membrane, which is dominated by the molecular chains of carbon and oxygen due to the use of organic polymers such as PVA and gelatin. In addition to being a natural polymer originating from porcine cartilage, gelatin is responsible for the calcium and silicon content in the membrane [41]. The iron content was detected in trace amounts, signifying the success of the synthesis process in forming a complex of oxygen atoms in the membrane structure [42]. Due to the imprinting of the membrane surface, the EDS detector does not detect any iron elements but confirms the presence of chlorine elements. This clearly showed the success of the process in removing iron content within membrane structures.

3.3. Crystallinity of membrane

The crystallinity of both membranes was observed by the diffraction pattern of XRD within the 2-theta angle range of 5°–60°, as shown in Figure 6. Both samples demonstrated an amorphous characteristic pattern with a maximum peak at about 20°, corresponding to the signature characteristics of PVA as well as gelatin diffraction patterns [43, 44].

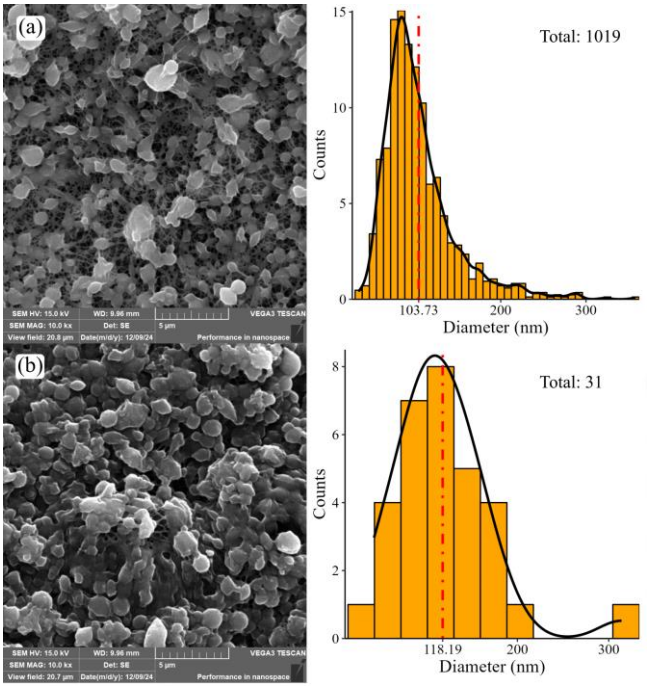

Figure 4 Morphology and fiber distribution of PVA/GE 15/5 wt.%~CA membrane: before (a) and after washed by HCl (b).

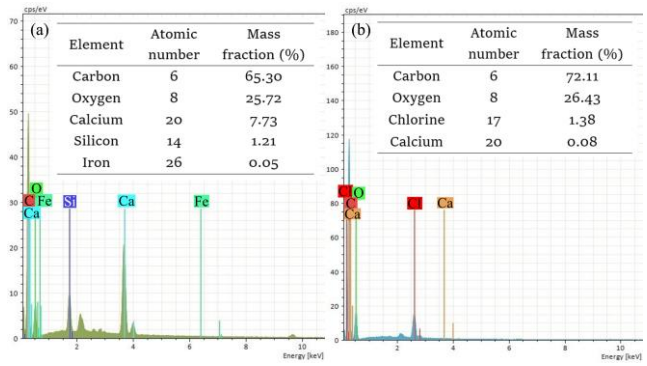

Figure 5 EDS spectra of PVA/GE 15/5 wt.%~CA membrane: before (a) and after washed by HCl (b).

 DOI: 10.15826/chimtech.2024.11.3.01

As proposed by Chen et al. [23], the crosslinking process adds more amorphous region to the polymeric structure, leading to low crystallinity of the membrane. However, the peak position barely shifted, signifying the inability of the imprinting process to shatter the structure of the polymer [45].

Peaks at 19.17° and 18.99° for HCl-treated and untreated membranes, respectively, correspond to the (200) plane of Fe_2O_3 (AMCSD code 0019940). This slight shift of peaks might be due to the extracted iron after HCl treatment leaving the structure of the polymer. In addition, the deconvolution peak of HCl-treated membrane is shown in Figure 7. The single peak is composed of three different peaks, which show a minor peak of gelatin at 16.44°, indicating a triple helix structure of gelatin [46, 47]. The highest peak at 21.73° corresponds to pure PVA as the main polymer used, and the trace content of Fe^{3+} is indicated by the peak at 26.08° [29].

3.4. Assessment of stability in water

Based on a macro perspective, the results of the chemical crosslinking process in the membrane were observed through the water resistance. This showed the stability of the membrane structure after interacting with water molecules or similar polar solvents. Assessment methods applied to assess stability against water are water contact angle (WCA) measurements and direct immersion tests.

Figure 8 shows the difference in the results of measuring the WCA for crosslinked and non-crosslinked fiber. Images were captured using a 5 MP camera set at macro configuration (f/2.4), and the WCA was measured using ImageJ version 1.54f with the plugin named Drop Analysis LB-ADSA (Low Bond Axisymmetric Drop Shape Analysis) [27, 48].

The results suggest that the crosslinking process has drastically increased the water resistance of the membrane, with improvements from 46° to 91° and 87° in CA and GA, respectively. This was attributed to the chemical interaction between the fiber molecular structure and the crosslinker agent, manifested in the resistance properties of the membrane [49]. Additionally, crosslinking by citric acid showed a better result compared to glutaraldehyde.

The immersion test was conducted by immersing the membrane sheet, which had been previously weighed (m), in water at room temperature for 24 h at 80 °C for an hour. Subsequently, the membrane was dried and weighed (m') to detect whether any structure was lost due to dissolution. The assessment was measured through the percentage of weight lost (w_l) [50], based on the following equation:

$$w_l = \frac{m - m'}{m} \cdot 100\%. \quad (1)$$

The immersion test provided that the membrane of CA-crosslinked lost a significant amount of mass compared to GA-crosslinked in both immersions at room temperature and 80 °C, as shown in Table 2.

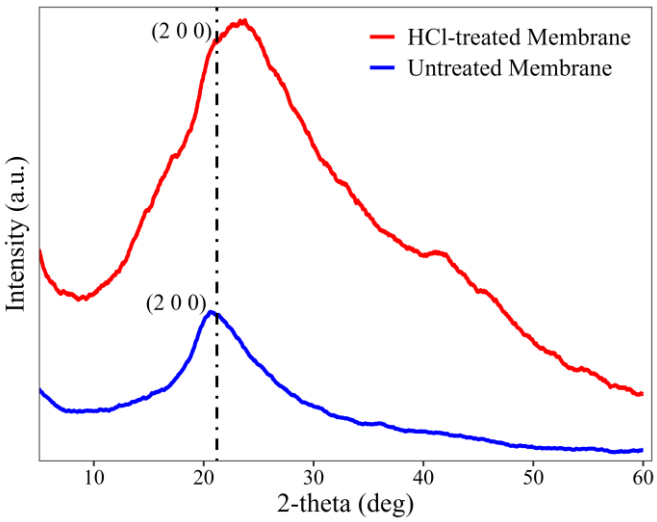

Figure 6 XRD patterns of PVA/GE 15/5 wt.%~CA membrane: without (red) and with HCl treatment (blue).

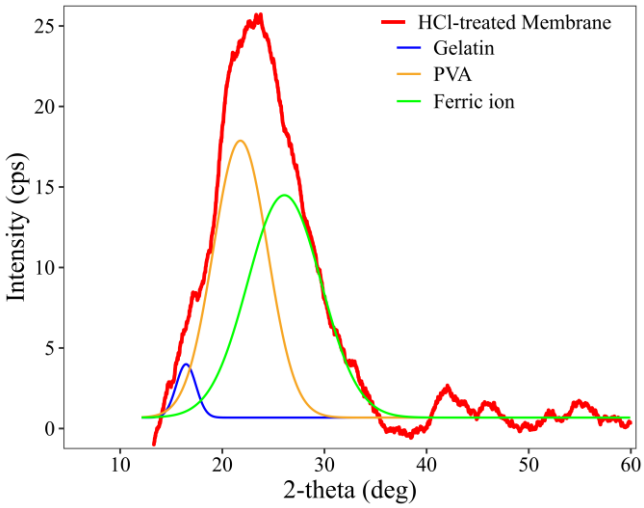

Figure 7 Deconvolution of HCl-treated membrane pattern.

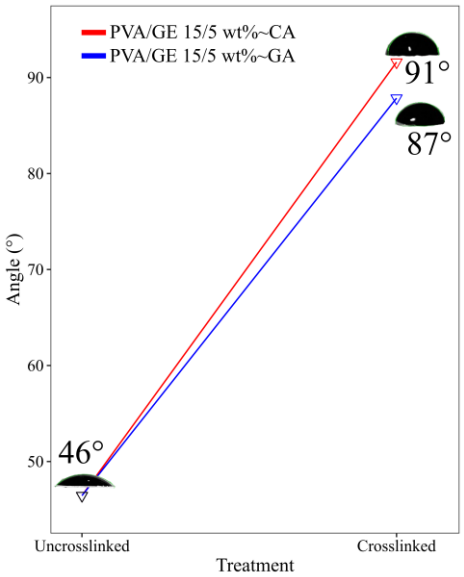

Figure 8 Measurement of water contact angle (WCA) on PVA/GE 15/5 wt.% membrane with CA- (red) and GA-crosslinked (blue).

 DOI: 10.15826/chimtech.2024.11.3.01

Table 2 Immersion test results.

Membrane(s)	Temp. (°C)	Weight lost
PVA/GE 15/5 wt.%	Room	100%
PVA/GE 15/5 wt.%-CA	Room	12.0%
	80	14.3%
PVA/GE 15/5 wt.%-GA	Room	7.7%
	80	8.2%

This weight loss is related to the hydroxyl content within both membranes, with PVA/GE 15/5 wt.%-CA membrane losing the most weight. Due to its reactivity, hydroxyl group could form water molecules with free hydrogen ions in water, resulting in the weight loss in the membrane [51]. Meanwhile, the uncrosslinked membrane dissolved completely at the point of contact with the water, losing 100% of its mass. It is acceptable that higher temperature causes more damage to the membrane due to fast movement of water molecule; however, the damage caused based on weight loss does not appear to be much different compared to immersion in room-temperature, and the membrane still retains most of its structure.

4. Limitations

Based on observations, the membrane was dominated by nanobead formation due to the low viscosity of the solution and the use of low-molecular-weight PVA. The high amino acid content of gelatin makes the functional groups of crosslinked products harder to examine. Therefore, future studies should focus on the synthesis of nanofiber membranes by higher molecular-weight PVA and the combination of other natural or synthetic polymers, with optimization both on electrospinning setup and crosslinking mechanisms. These include investigations on heating temperature variation, time exposure, and/or the effect of combination crosslinkers.

5. Conclusions

The approach of different crosslinking mechanisms was applied to achieve water-resistant PVA/GE 15/5 wt.% membranes synthesized using the electrospinning method. The macro assessment concluded that the membrane exhibits water-resistant properties, as shown by a significant increase in the water contact angle after the crosslinking process, measured at 91° and 87° for citric acid (CA)-crosslinked and glutaraldehyde (GA)-crosslinked membranes. The water immersion test comes to the same conclusion. The percentage of weight loss happens to be quite low in GA-crosslinked membrane compared to CA-crosslinked membrane, measured at 7.7% and 12%, respectively. This indicates that the membranes remain intact when immersed, in contrast to the uncrosslinked membrane which readily dissolves. Micro assessment with FTIR characterization showed that each crosslinking agent successfully conducted its crosslinking mechanism, namely acetalization by GA and esterification by CA, confirming a new band at ~1700 cm^{-1} for both mechanisms. Morphology of the membranes by SEM imaging confirmed the formation of nanobeads and nanofibers, where the deformed structure slightly shifted the average fiber diameter from 103 nm to 118 nm due to the effect of the imprinting process. Furthermore, HCl imprinted iron sites on the surface of the membrane, signified by undetected iron elements by EDS characterization. It is important to acknowledge that XRD characterization confirmed the amorphous region of the membranes, with the crystal phase of Fe_2O_3 at ~19° 2θ angle. The results provide significant insights into possible mechanisms to achieve water-resistant properties of membrane to unfold the potency of reusability and efficiency in water treatment.

• Supplementary materials

No supplementary materials are available.

• Funding

The research/publication of this article was funded by University of Sriwijaya Unggulan Kompetitif grant 2024 in accordance to Rector's decree Number 0013/UN9/SK.LP2M.PT/2024 dated May 20th 2024.

• Acknowledgments

We acknowledg the Institute for Research and Community Service of Sriwijaya University (LPPM UNSRI) for funding and supporting this research. Also, we show our deepest gratitude to the Laboratory of Material Science for facilitating the research.

• Author contributions

Conceptualization: I.A., I.R., F.M.
Data curation: I.A., I.R.
Formal Analysis: I.A., I.R.
Funding acquisition: I.R., E.K., J., O.C.S.
Methodology: I.A., I.R., J.
Project administration: E.K., J., O.C.S.
Resources: I.R., E.K., J., O.C.S.
Software: I.A., F.M.
Supervision: I.R., F.M.
Validation: I.R., F.M.
Visualization: I.A.
Writing – original draft: I.A., I.R., F.M.
Writing – review & editing: I.A., I.R., F.M.

• Conflict of interest

The authors declare no conflict of interest.

• Additional information

Authors IDs:
Idha Royani, Scopus ID 56070235100;

 DOI: 10.15826/chimtech.2024.11.3.01

Fiber Monado, Scopus ID 55330195600;
Erry Koriyanti, Scopus ID 57190016099;
Jorena, Scopus ID 57219119084;
Octavianus Cakra Satya, Scopus ID 57190934843;

Website:
University of Sriwijaya, https://www.unsri.ac.id/.

References

1. Tran HD, Nguyen DQ. Study on methylene blue adsorption using cashew nut shell-based activated carbon. Chim Tech Acta. 2023;10(4):202310401. doi:10.15826/chimtech.2023.10.4.01
2. Srivastav AL, Patel N, Chaudhary VK. Disinfection by-products in drinking water: Occurrence, toxicity and abatement. Environ Pollut. 2020;267:115474. doi:10.1016/j.envpol.2020.115474
3. Edianta J, Satya OC, Virgo F, Saleh K, Royani I. Design of potentiometric instrumentation system based on Arduino nano microcontroller using imprinted polymer for the determination of Fe (III) metal ions. AIP Conf Proc. 2023;120007. doi:10.1063/5.0125919
4. Li C, Yang L, Shi M, Liu G. Persistent organic pollutants in typical lake ecosystems. Ecotoxicol Environm Safety. 2019;180:668–678. doi:10.1016/j.ecoenv.2019.05.060
5. Chheang L, Thongkon N, Sriwiriyarat T, Thanasupsin SP. Heavy Metal Contamination and Human Health Implications in the Chan Thnal Reservoir, Cambodia. Sustainability. 2021;13(24):1–20. doi:10.3390/su132413538
6. Ugaz CAV, León-Roque N, Nuñez-León JL, Hidalgo-Chávez DW, Oblitas J. Geochemical and environmental assessment of potential effects of trace elements in soils, water, and sediments around abandoned mining sites in the northern Iberian Peninsula (NW Spain). Heliyon. 2023;9(3):1–11. doi:10.1016/j.heliyon.2023.e14659
7. Kamarati K, Ivanhoe M, Sumaryono M. Kandungan Logam Berat Besi (Fe), Timbal (Pb). dan Mangan (Mn) pada Air Sungai Santan [Heavy Metal Content Iron (Fe), Lead (Pb) and Manganese (Mn) in The Water of The Santan River]. J Penelitian Ekosistem Dipterokarpa. 2018;4(1):49–56. doi:10.20886/jped.2018.4.1.49-56
8. World Health Organization. Guidelines for Drinking-water Quality. 3rd ed. Geneva: World Health Organization. 2008; 668 p.
9. Rusydi AF, Onodera SI, Saito M, Ioka S, Maria R, Ridwansyah I, et al. Vulnerability of groundwater to iron and manganese contamination in the coastal alluvial plain of a developing Indonesian city. SN Appl Sci. 2021;3(4):12. doi:10.1007/s42452-021-04385-y
10. Raji Z, Karim A, Karam A, Khalloufi S. Adsorption of Heavy Metals: Mechanisms, Kinetics, and Applications of Various Adsorbents in Wastewater Remediation—A Review. Waste. 2023;1(3):775–805. doi:10.3390/waste1030046
11. Royani I, Maimunah M, Edianta J, Alfikro I, Monado F, Jorena J, et al. Synthesis of Ion Imprinted Polymers (IIPs) Adsorbent Materials Using Fe(III) Leaching Process with Variation of Hydrochloric Acid Solvent Concentration and Heat Treatment. Sci Technol Indones. 2024;9(2):336–344. doi:10.26554/sti.2024.9.2.336-344
12. Novianty N, Edianta J, Jorena J, Saleh K, Bama AA, Koriyanti E, et al. Synthesis of Fe(III)-IIPs (Ion Imprinted Polymers): Comparing Different Concentrations of HCl and HNO_3 Solutions in the Fe(III) Polymer Extraction Process for Obtaining the Largest Cavities in Fe(III)-IIPs. Sci Technol Indones. 2023;8(3):361–366. doi:10.26554/sti.2023.8.3.361-366
13. Ye S, Zhang W, Hu X, He H, Zhang Y, Li W, et al. Selective Adsorption Behavior and Mechanism for Cd(II) in Aqueous Solution with a Recoverable Magnetie-Surface Ion-Imprinted Polymer. Polymers. 2023;15(11):1–23. doi:10.3390/polym15112416
14. Aljohani MS, Alnoman RB, Alharbi HY, Al-Anazia M, Monier M. Designing of a cellulose-based ion-imprinted biosorbent for selective removal of lead(II) from aqueous solutions. Int J Biol Macromolec. 2024;259(129145):1–14. doi:10.1016/j.ijbiomac.2023.129145
15. Çıtlakoğlu M, Yolcu Z. Dinuclear Pb(II) monomer complex: Synthesis, characterization, and application of Pb(II) ion-imprinted polymer as a selective potentiometric microsensor. Polyhedron. 2023;243(116539):1-10. doi:10.1016/j.poly.2023.116539
16. Zhao R, Li X, Sun B, Li Y, Li Y, Wang C. Preparation of molecularly imprinted sericin/poly(vinyl alcohol) electrospun fibers for selective removal of methylene blue. Chem Res Chin Univ. 2017;33(6):986–994. doi:10.1007/s40242-017-7115-9
17. Li Y, Zhang J, Xu C, Zhou Y. Crosslinked chitosan nanofiber mats fabricated by one-step electrospinning and ion-imprinting methods for metal ions adsorption. Sci China Chem. 2016;59(1):95–105. doi:10.1007/s11426-015-5526-3
18. Kanu NJ, Gupta E, Vates UK, Singh GK. Electrospinning process parameters optimization for biofunctional curcumin/gelatin nanofibers. Mater Res Express. 2020;7(3):1–27. doi:10.1088/2053-1591/ab7f60
19. Ahmadijokani F, Molavi H, Bahi A, Wuttke S, Kamkar M, Rojas OJ, et al. Electrospun nanofibers of chitosan/polyvinyl alcohol/UiO-66/nanodiamond: Versatile adsorbents for wastewater remediation and organic dye removal. Chem Engineering J. 2023;457(141176):1–12. doi:10.1016/j.cej.2022.141176
20. Maksotova KS, Kalikh DT, Omirzakova AT, Bakirova BS, Akbayeva DN. Polymer-metal complex based on copper(II) acetate and polyvinyl alcohol: thermodynamic and catalytic properties. Chim Tech Acta. 2022;9(3):20229304;6015. doi:10.15826/chimtech.2022.9.3.04
21. Song M, Yu H, Gu J, Ye S, Zhou Y. Chemical cross-linked polyvinyl alcohol/cellulose nanocrystal composite films with high structural stability by spraying Fenton reagent as initiator. Int J Biol Macromolec. 2018;113:171–178. doi:10.1016/j.ijbiomac.2018.02.117
22. Zanini S, Papagni A, Vaghi L, Kaur Thatti B, Barton S, Williams N, et al. Sulfur Hexafluoride (SF_6) Plasma Treatment of Medical Grade Poly(methyl methacrylate). Coatings. 2020;10(2):1–14. doi:10.3390/coatings10020135
23. Chen W, Gao Z, He M, Dou Y, Yin G, Ding J. Vapor-phase glutaraldehyde crosslinked waste protein-based nanofiber nonwovens as an environmentally friendly wound dressing. Reactive and Functional Polymers. 2022;172(105203):1–9. doi:10.1016/j.reactfunctpolym.2022.105203
24. Czibulya Z, Csík A, Tóth F, Pál P, Csarnovics I, Zelkó R, et al. The Effect of the PVA/Chitosan/Citric Acid Ratio on the Hydrophilicity of Electrospun Nanofiber Meshes. Polymers. 2021;13(20):1–18. doi:10.3390/polym13203557
25. Jeong S, Oh SG. Antiacne Effects of PVA/ZnO Composite Nanofibers Crosslinked by Citric Acid for Facial Sheet Masks. Xiao H, editor. Int J Polymer Sci. 2022;2022:1–7. doi:10.1155/2022/4694921
26. Döbelin N, Archer R, Tu V. A free and open-source solution for Rietveld refinement of XRD data from the CheMin instrument onboard the Mars rover Curiosity. Planetary Space Sci. 2022;224(105596):1-13. doi:10.1016/j.pss.2022.105596
27. Stalder AF, Melchior T, Müller M, Sage D, Blu T, Unser M. Low-bond axisymmetric drop shape analysis for surface tension and contact angle measurements of sessile drops. Colloids and Surfaces A: Physicochemical and Engineering Aspects. 2010;364(1–3):72–81. doi:10.1016/j.colsurfa.2010.04.040
28. Felix CSA, Chagas AVB, De Jesus RF, Barbosa WT, Barbosa JDV, Ferreira SLC, et al. Synthesis and Application of a New Polymer with Imprinted Ions for the Preconcentration of Uranium in Natural Water Samples and Determination by Digital

Imaging. Molec. 2023;28(10):1–15. doi:10.3390/molecules28104065
29. Sun M, Wang Y, Yao L, Li Y, Weng Y, Qiu D. Fabrication and Characterization of Gelatin/Polyvinyl Alcohol Composite Scaffold. Polymers. 2022;14(7):1-14. doi:10.3390/polym14071400
30. Zheng W, Sun C, Bai B. Molecular Dynamics Study on the Effect of Surface Hydroxyl Groups on Three-Phase Wettability in Oil-Water-Graphite Systems. Polymers. 2017;9(8):1–9. doi:10.3390/polym9080370
31. Huang SM, Liu SM, Tseng HY, Chen WC. Effect of Citric Acid on Swelling Resistance and Physicochemical Properties of Post-Crosslinked Electrospun Polyvinyl Alcohol Fibrous Membrane. Polymers. 2023;15(7):1–13. doi:10.3390/polym15071738
32. Perez-Puyana V, Jiménez-Rosado M, Romero A, Guerrero A. Development of PVA/gelatin nanofibrous scaffolds for Tissue Engineering via electrospinning. Mater Res Express. 2018;5(3):1–8. doi:10.1088/2053-1591/aab164
33. Li M, Guo L, Mu Y, Huang X, Jin L, Xu Q, et al. Gelatin films reinforced by tannin-nanocellulose microgel with improved mechanical and barrier properties for sustainable active food packaging. Food Hydrocolloids. 2024;149(109642):1–11. doi:10.1016/j.foodhyd.2023.109642
34. Etxabide A, Akbarinejad A, Chan EWC, Guerrero P, De La Caba K, Travas-Sejdic J, et al. Effect of gelatin concentration, ribose, and glycerol additions on the electrospinning process and physicochemical properties of gelatin nanofibers. European Polymer Journal. 2022;180(111597):1–11. doi:10.1016/j.eurpolymj.2022.111597
35. Kumar A, Ryparová P, Hosseinpourpia R, Adamopoulos S, Prošek Z, Žigon J, et al. Hydrophobicity and resistance against microorganisms of heat and chemically crosslinked poly(vinyl alcohol) nanofibrous membranes. Chemical Engineering Journal. 2019;360:788–796. doi:10.1016/j.cej.2018.12.029
36. Huang CY, Hu KH, Wei ZH. Comparison of cell behavior on PVA/PVA-Gelatin electrospun nanofibers with random and aligned configuration. Sci Rep. 2016;6(37960):1-8. doi:10.1038/srep37960
37. Klein DR. Organic Chemistry. 4th ed. Hoboken: John Wiley & Sons; 2021. 1302 p.
38. Yagizatli Y, Sahin A, Ar I. Effect of thermal crosslinking process on membrane structure and PEM fuel cell applications performed with SPEEK-PVA blend membranes. International J Hydrogen Energy. 2022;47(95):40445–40461. doi:10.1016/j.ijhydene.2022.04.183
39. Nandiyanto ABD, Ragadhita R, Fiandini M. Interpretation of Fourier Transform Infrared Spectra (FTIR): A Practical Approach in the Polymer/Plastic Thermal Decomposition. Indonesian J Sci Technol. 2022;8(1):113–126. doi:10.17509/ijost.v8i1.53297
40. Vatanpour V, Kose-Mutlu B, Koyuncu I. Electrospraying technique in fabrication of separation membranes: A review. Desalination. 2022;533(115765):1-17. doi:10.1016/j.desal.2022.115765
41. Zhang H, Liu Z, Zhang J, Zhang L, Wang S, Wang L, et al. Identification of Edible Gelatin Origins by Data Fusion of NIRS, Fluorescence Spectroscopy, and LIBS. Food Anal Methods. 2021;14(3):525–536. doi:10.1007/s12161-020-01893-2
42. Cao Y, Hu X, Zhu C, Zhou S, Li R, Shi H, et al. Sulfhydryl functionalized covalent organic framework as an efficient adsorbent for selective Pb(II) removal. Colloids and Surfaces A: Physicochemical and Engineering Aspects. 2020;600(125004):1-8. doi:10.1016/j.colsurfa.2020.125004
43. Ahlawat J, Kumar V, Gopinath P. Carica papaya loaded poly (vinyl alcohol)-gelatin nanofibrous scaffold for potential application in wound dressing. Mater Sci Engin C. 2019;103(109834):1–9. doi:10.1016/j.msec.2019.109834
44. Pandey VK, Upadhyay SN, Niranjan K, Mishra PK. Antimicrobial biodegradable chitosan-based composite Nano-layers for food packaging. Int J Biol Macromolec. 2020;157(1):212–219. doi:10.1016/j.ijbiomac.2020.04.149
45. He W, Yu Q, Wang N, Ouyang X kun. Efficient adsorption of Cu(II) from aqueous solutions by acid-resistant and recyclable ethylenediamine tetraacetic acid-grafted polyvinyl alcohol/chitosan beads. J Molecular Liquids. 2020;316(113856):1–10. doi:10.1016/j.molliq.2020.113856
46. Suderman N, Isa MIN, Sarbon NM. Characterization on the mechanical and physical properties of chicken skin gelatin films in comparison to mammalian gelatin films. IOP Conf Ser: Mater Sci Eng. 2018;440:1–12. doi:10.1088/1757-899X/440/1/012033
47. Mosleh Y, De Zeeuw W, Nijemeisland M, Bijleveld JC, Van Duin P, Poulis JA. The Structure–Property Correlations in Dry Gelatin Adhesive Films. Adv Eng Mater. 2021;23(1):1–9. doi:10.1002/adem.202000716
48. Hartig SM. Basic Image Analysis and Manipulation in ImageJ. Curr Protocols Molecular Biol. 2013;102(1):1–12. doi:10.1002/0471142727.mb1415s102
49. Ding J, Chen M, Chen W, He M, Zhou X, Yin G. Vapor-Assisted Crosslinking of a FK/PVA/PEO Nanofiber Membrane. Polymers. 2018;10(7):747–757. doi:10.3390/polym10070747
50. Miraftab M, Saifullah AN, Çay A. Physical stabilisation of electrospun poly(vinyl alcohol) nanofibres: comparative study on methanol and heat-based crosslinking. J Mater Sci. 2015;50(4):1943–1957. doi:10.1007/s10853-014-8759-1
51. Hulupi M, Haryadi H. Synthesis and Characterization of Electrospinning PVA Nanofiber-Crosslinked by Glutaraldehyde. Mater Today Proc 2019;13:199–204. doi:10.1016/j.matpr.2019.03.214